Elastic response of binary hard-sphere fluids

J. M. Rickman[1,2] and H. Daniel Ou-Yang[2]
[1]*Department of Materials Science and Engineering*
[2]*Department of Physics, Lehigh University, Bethlehem, Pennsylvania 18015, USA*
(Received 30 March 2011; revised manuscript received 25 May 2011; published 25 July 2011)

We derive expressions for the high-frequency, wave-number-dependent elastic constants of a binary hard-sphere fluid and employ Monte Carlo computer simulation to evaluate these constants in order to highlight the impact of composition and relative sphere diameter on the elastic response of this system. It is found that the elastic constant $c_{11}(k)$ exhibits oscillatory behavior as a function of k whereas the high-frequency shear modulus, for example, does not. This behavior is shown to be dictated by the angular dependence (in $\vec{k}$ space) of derivatives of the interatomic force at contact. The results are related to recent measurements of the compressibility of colloidal fluids in laser trapping experiments.

DOI: 10.1103/PhysRevE.84.012401 PACS number(s): 61.20.Ja, 62.10.+s

I. INTRODUCTION

The determination of the mechanical properties of simple liquids has been of interest for many years. In particular, the calculation of these properties provides a testbed for the machinery of the statistical mechanics of fluids, especially analytical approximations to correlation functions. For example, Venkatesh and Gopala Rao [1] have computed the interatomic potential for liquid selenium employing the Percus-Yevick [2] and hypernetted-chain equations with experimental diffraction data as input. This potential was then used to obtain the elastic constants of the liquid for comparison with other calculations and experiment. In the same time period, Khajil [3] employed an analytic pair potential that incorporates transition-metal d-band effects to compute the elastic properties of liquid platinum and chromium.

Recent experimental advances now permit the determination of the elastic response of fluids over a range of wavelengths via laser trapping. Indeed, recent experiments on binary fluids using optical traps have shown that one can determine the dependence of the isothermal compressibility of confined nanoparticles on their size and number density from measured changes in the number of trapped particles [4]. The interpretation of such compressibility data is difficult, however, given limited information on the details of colloidal interaction. The elastic constants of the fluid are, however, a probe of depletion forces that are associated with effective, entropic interactions that result from an imbalance in osmotic pressure [5]. The first quantitative model of these interactions, based on an excluded-volume model, was developed by Asakura and Oosawa [6] and has been subsequently investigated and refined by many others [7–9].

In this paper we compute the high-frequency, finite-wavelength elastic constants of the fluid using relations developed by Schofield linking stress correlations to partial radial distribution functions [10]. Monte Carlo simulation is employed to calculated the radial distribution functions and the expressions for the elastic constants are used to quantify the impact of composition and relative sphere diameter on the bulk modulus over a range of wavelengths. For simplicity, we focus here on the binary hard-sphere fluid, the quintessential athermal system in which entropic interactions dictate structure and properties and can lead, in some cases, to entropic phase transitions [11]. As will be seen below, one advantage of employing a hard-sphere interaction is that analytical expressions for the elastic constants can be developed for this system that provide insight into its mechanical response over a wide range of wavelengths. Such expressions will facilitate the interpretation of experimental compressibility data. We note that this system also serves as a model for the study of more realistic and hence more complex mixtures, including colloidal mixtures [12]. Nevertheless, despite its simplicity, the binary hard-sphere fluid also embodies the essential ingredients of the depletion interaction.

II. ELASTIC PROPERTIES

Consider first a monatomic fluid. Several years ago Schofield derived expressions for the Fourier transform of the high-frequency, local elastic constants of such a fluid [10]. Postulating a linear relationship between the components of the stress rate $\dot{\sigma}_{\alpha\beta}(\vec{k})$ and the strain rate $\epsilon_{\mu\delta}(\vec{k})$ in reciprocal (i.e., $\vec{k}$) space, he first defined the components of the wavelength-dependent elastic constant tensor $C_{\alpha\beta\mu\delta}(\vec{k})$ via the constitutive relation

$$\dot{\sigma}_{\alpha\beta}(\vec{k}) = C_{\alpha\beta\mu\delta}(\vec{k})\epsilon_{\mu\delta}(\vec{k}) + \dot{\sigma}'_{\alpha\beta}(\vec{k}), \tag{1}$$

where the primed reference stress is orthogonal to the strain, the overdot denotes a time derivative, and the Einstein summation convention is employed for notational convenience. If the focus is on high-frequency elastic behavior, then elastic constants can be defined in terms of static correlations involving the radial distribution function. In particular, by correlating Eq. (1) with the strain rate and employing the stationary property of correlation functions, it can then be shown that the elastic constants for a monatomic liquid having a density ρ with interactions given by a pair potential $u(r)$ are given in terms of the radial distribution function $g(r)$ by the stress-stress correlation functions [13]

$$\begin{aligned} c_{11}(k) &= \beta\langle\sigma_{zz}(\vec{k})\sigma_{zz}(-\vec{k})\rangle \\ &= \rho\left[\frac{3}{\beta} + \rho\int d^3r\, g(r)\frac{\partial^2 u}{\partial z^2}\left(\frac{1-\cos kz}{k^2}\right)\right], \\ c_{12}(k) &= \beta\langle\sigma_{zz}(\vec{k})\sigma_{xx}(-\vec{k})\rangle \end{aligned}$$

$$= \rho\left[\frac{1}{\beta} + \rho\int d^3r\, g(r)\left(\frac{x}{z}\frac{\partial^2 u}{\partial x\partial z} - \frac{x}{z^2}\frac{\partial u}{\partial x}\right) \times \left(\frac{1-\cos kz}{k^2}\right)\right],$$

$$c_{44}(k) = \beta\langle\sigma_{xy}(\vec{k})\sigma_{xy}(-\vec{k})\rangle = \rho\left[\frac{1}{\beta} + \rho\int d^3r\, g(r)\frac{\partial^2 u}{\partial x^2}\left(\frac{1-\cos kz}{k^2}\right)\right], \quad (2)$$

where the angular brackets denote an equilibrium average, β is the inverse temperature, the z axis is taken along the direction of $\vec{k}$, and standard Voigt notation for the elastic constants (i.e., $C_{1111} = c_{11}$, etc.) has been introduced. These expressions have already been employed to determine the elastic constants of a Lennard-Jones fluid using computer simulation [14]. Our first aim here is to generalize these results to obtain tractable expressions for the elastic constants of a binary, hard-sphere fluid.

This generalization can be made by noting that the relevant quantities for hard-sphere systems are related to radial distribution functions at sphere contact. Thus the integrals in Eqs. (2) can be written in terms of $g(r)u'(r) = -(1/\beta)y(r)\,d\exp[-\beta u(r)]/dr$, where $y(r)$ is the cavity distribution function [15], prime denotes spatial differentiation, and $g(r)u''$. For the hard-sphere potential with sphere diameter σ, one finds that $g(r)u'(r) = -(1/\beta)y(\sigma^+)\delta(r-\sigma)$ [15], where $\delta(r)$ is the Dirac delta function, and that $g(r)u''(r) = (-1/\beta)d[y(r)\delta(r-\sigma)]/dr - y(r)w'(r)\delta(r-\sigma)$, where $w(r)$ is the potential of mean force. It should be noted that since $g(r) = \exp[-\beta w(r)] = y(r)\exp[-\beta u(r)]$, then, since $y(r)$ is continuous, $y(\sigma) = g(\sigma^+)$.

Equations (2) can then be written in terms of $g(\sigma^+)$ and $w'(\sigma^+)$ as

$$\bar{c}_{11}(k) = 3\bar{\rho} + \left(\frac{2\pi\bar{\rho}^2}{\bar{k}^2}\right)g(\sigma^+)\left\{-I_2(\bar{k}) - \frac{1}{2}\beta\sigma w'(\sigma^+)I_1(\bar{k}) + [2I_1(\bar{k}) + \bar{k}I_1'(\bar{k})]\right\},$$

$$\bar{c}_{12}(k) = \bar{\rho} + \left(\frac{\pi\bar{\rho}^2}{\bar{k}^2}\right)g(\sigma^+)\left\{-I_4(\bar{k}) - \frac{1}{2}\beta\sigma w'(\sigma^+)I_2(\bar{k}) + [2I_2(\bar{k}) + \bar{k}I_2'(\bar{k})]\right\},$$

$$\bar{c}_{44}(k) = \bar{\rho} + \left(\frac{\pi\bar{\rho}^2}{\bar{k}^2}\right)g(\sigma^+)\left\{-I_3(\bar{k}) - \frac{1}{2}\beta\sigma w'(\sigma^+)I_2(\bar{k}) + [2I_2(\bar{k}) + \bar{k}I_2'(\bar{k})]\right\}, \quad (3)$$

where $\bar{c}_{ij} = \beta c_{ij}\sigma^3$, $\bar{\rho} = \rho\sigma^3$, and $\bar{k} = k\sigma$; the functions I_i ($i = 1,2,3,4$) are evaluated in the Appendix. It should be noted that, in general, the fluid is elastically isotropic only for $\vec{k} = \vec{0}$, as evidenced by the vanishing of the anisotropy parameter $\bar{c}_{11}(\bar{k}) - \bar{c}_{12}(\bar{k}) - 2\bar{c}_{44}(\bar{k})$ in this limit [13]. Finally, the corresponding expressions for a multicomponent fluid can be obtained upon making the substitution [16] $g(r) \to \sum_{i,j} x_i x_j g_{ij}(r_{ij})$, where x_i is the composition of the ith component, $g_{ij}(r_{ij})$ are the partial radial distribution functions with species i and j separated by r_{ij}, and $g(r)$ is then defined as the total correlation function [17].

III. SIMULATION METHODOLOGY

In our Monte Carlo simulations of a binary, hard-sphere liquid, two spherical particles α and β interacted via the additive hard-sphere potential [18] in which $d_{ij} = (d_{ii} + d_{jj})/2$ is the hard-sphere diameter. For concreteness, take 1 (2) to denote the larger (smaller) spheres. The simulations began with N larger spheres, each having a diameter σ, located on the sites of a face-centered-cubic lattice with M unit cells on a side, each cell having a lattice parameter ℓ. The n smaller spheres, each having a diameter $\alpha\sigma$, were located at a fraction of the octahedral interstices of the lattice. Thus $d_{11} = \sigma, d_{12} = d_{21} = \sigma(1+\alpha)/2$, $d_{22} = \alpha\sigma$, and $\bar{d}_{ij} = d_{ij}/\sigma$. The corresponding reduced number density $\bar{\rho} = \rho\sigma^3 = (N+n)\sigma^3/M^3\ell^3$ and composition $x = n/(N+n)$.

Given this starting configuration, the simulation procedure is the standard Metropolis Monte Carlo algorithm applied to hard spheres in a spatially periodic simulation cell. It should be noted that for highly asymmetric systems (i.e., $\alpha \lesssim 0.1$) long runs may be needed to ensure proper sampling [12]. In this work we restrict our attention to $\alpha > 0.3$ and monitor the displacements of the spheres to verify that particles move several times σ over the course of a run. Simulation runs consisting of from 1×10^5 to 2×10^5 Monte Carlo steps were used to obtain pair-correlation functions that are central to our calculations of finite-wavelength elastic properties.

IV. SIMULATION RESULTS

Simulations were carried out in the liquid state, as determined by previous calculations of the phase diagram for particular values of the total pressure and x [12]. Consider first the binary liquid for $\alpha = 0.414$ for a range of compositions x. In our simulations we used $N = 500$ large spheres and varied n to achieve the desired composition.

Figure 1 shows the corresponding partial radial distribution functions $g_{ij}(r)$ $(i,j = 1,2)$ for $x = 0.34$ and the calculated

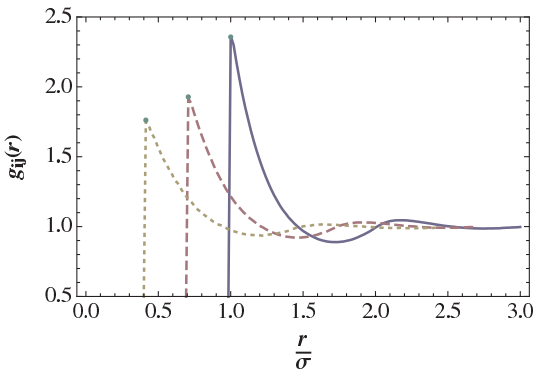

FIG. 1. (Color online) Partial radial distribution functions $g_{11}(r)$ (solid curve), $g_{22}(r)$ (dotted curve), and $g_{12}(r)$ (dashed curve) for $\alpha = 0.414$, $x = 0.339$, and $\bar{\rho} = 0.779$. The corresponding values for $g_{ij}(d_{ij})$, calculated using the Carnahan-Starling result [19], are also shown (dots).

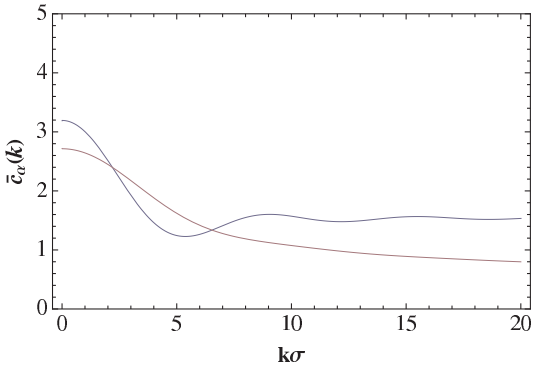

FIG. 2. (Color online) Normalized elastic constants $\bar{c}_\alpha(k)$ versus normalized wave number $k\sigma$ for a monocomponent hard-sphere fluid with $\bar{\rho} = 0.52$. The curves, starting with the topmost curve, correspond to $\alpha = 11$ and 12, respectively. Note the oscillations in $\bar{c}_{11}$ that are absent in the other constant.

values for $g_{ij}(d_{ij})$ using a linear combination of solutions to the Percus-Yevick equation, an approximation that was also obtained by Carnahan and Starling [18,19]. As can be seen from the figure, the agreement between the values for the partial radial distribution functions at contact obtained via simulation and theory is excellent. These distribution functions were also used to verify that the total pressure of the system is in good agreement with that calculated from the Percus-Yevick equation.

The radial distribution function(s) can be employed to calculate the elastic properties of the hard-sphere liquid. For reference, consider first the finite-wavelength elastic constants for a monocomponent hard-sphere fluid with a density $\bar{\rho} = 0.52$, as calculated using Eqs. (3). For the purposes of illustration, Fig. 2 shows the normalized elastic constants $\bar{c}_{11}(k)$ and $\bar{c}_{12}(k)$ versus normalized wave number $k\sigma$. As discussed below, a linear combination of these two elastic constants yields the high-frequency bulk modulus that is the focus of this study. [The remaining elastic constant $\bar{c}_{44}(k)$ is a high-frequency, wave-number-dependent shear modulus whose zero-frequency counterpart vanishes [13].] From the figure it is evident that $\bar{c}_{11}(k)$ exhibits oscillatory behavior and that the other does not. This behavior is due largely to contributions from terms involving $u''(r)$ and, in particular, the derivative $I_1'(\bar{k})$ More specifically, as discussed in the Appendix, the oscillations occur due to the undamped asymptotic dependence of the term $\bar{k}I_1'(\bar{k}) \sim -2\cos\bar{k}$ found in Eqs. (3). Thus, from Eq. (A2), the wavelength of the (damped) oscillations is set by $k\sigma \approx \pi$. Similar oscillatory behavior for $\bar{c}_{11}(k)$ has also been noted for the Lennard-Jones fluid [14].

The elastic constants for a binary, hard-sphere fluid can be calculated by replacing the pair-correlation function used in the monocomponent case with the total (weighted) pair-correlation function, as described in Sec. II. The resulting elastic constant curves are qualitatively similar to those for the monocomponent case (see Fig. 2) and so they will not be reproduced here. In particular, $\bar{c}_{11}(k)$ also exhibits oscillatory behavior for the binary system, though the oscillations are somewhat less pronounced than those found in the case of a monocomponent fluid. In this case, the dependence of $\bar{c}_{11}$ on wave number is dictated by the interplay of three normalized wave numbers, namely, $k\sigma$, $k\sigma\alpha$, and $k\sigma(1+\alpha)/2$, corresponding to the three contact distances in this system. The superposition of these oscillations therefore results in some destructive interference and hence smaller amplitude oscillations.

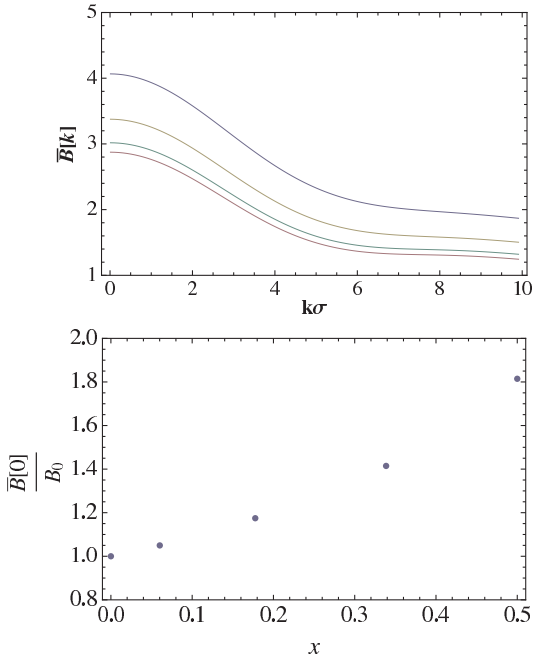

FIG. 3. (Color online) (a) The normalized, infinite-wavelength bulk modulus, $\bar{B}(k)$, versus the normalized wavenumber, $k\sigma$, with $\alpha = 0.414$. The curves, from top to bottom, correspond to the compositions $x = 0.339$, 0.178, 0.060, and 0.0, respectively. (b) The normalized, infinite-wavelength bulk modulus, $\bar{B}(\bar{k} = 0)/B_0$, where B_0 is the corresponding modulus for $x = 0$, versus composition, x, for a binary hard-sphere fluid with $\alpha = 0.414$.

To understand the impact of composition on elastic response, it is useful to focus on a single parameter, namely, the (normalized) wave-number-dependent bulk modulus given by $\bar{B}(\bar{k}) = [\bar{c}_{11}(k) + 2\bar{c}_{12}(k)]/3$. In the aforementioned laser trapping experiments [4], the dependence of the long-wavelength bulk modulus on composition has

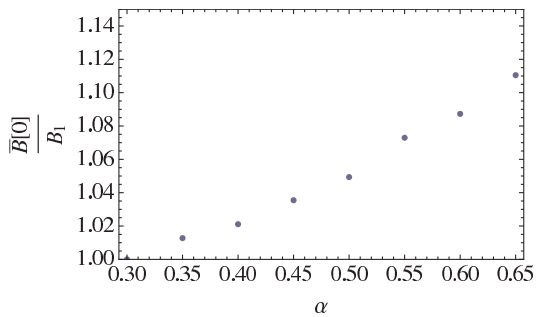

FIG. 4. (Color online) The normalized, infinite-wavelength bulk modulus, $\bar{B}(\bar{k} = 0)/B_1$ for $x = 0.178$, where B_1 is the corresponding modulus for $\alpha = 0.3$, versus the relative atomic diameter, α.

been studied and analyzed in terms of hard-sphere and other models. Thus we present in Fig. 3(a) the dependence of $\bar{B}(k)$ on $k\sigma$. This quantity, which depends also on $c_{12}(k)$, does not exhibit oscillatory behavior and indicates that the compressibility is higher at shorter length scales. Figure 3(b) shows the dependence of $\bar{B}(\bar{k}=0)$ on the composition x. Clearly, as the composition increases $\bar{B}$ increases as a greater excluded volume correlates with increases in $g_{ij}(d_{ij})$ and therefore a decrease in the attendant compressibility. Finally, consider the dependence of the bulk modulus on relative sphere diameter α, as shown in Fig. 4. As is evident from the figure, the bulk modulus increases upon increasing α, as would be expected intuitively.

V. DISCUSSION

The foregoing development can aid in the interpretation of the elastic properties of colloidal fluids obtained using the laser trapping experiments mentioned above [4]. In these experiments, elastic properties such as the compressibility are determined by monitoring local fluctuations in particle number. Thus an experimental determination of the dependence of the compressibility (i.e., inverse bulk modulus) on the composition and the relative ionic radii can be compared with the results obtained above [see Figs. 3(b) and 4] to ascertain over what range of composition a hard-sphere model is appropriate. Moreover, as the expressions obtained above Eqs. (3) permit one to define partial elastic constants by including only some of the radial distribution functions, one can make contact with experimental results involving fluctuations in the number of only one species.

Our results also suggest some useful extensions of the laser trapping experiments. For example, as one can calculate the dependence of the bulk modulus on wave number, it would be helpful to obtain k-dependent information from the experiments in order to extract additional thermodynamic information (e.g., potentials of mean force). This might be accomplished by employing a range of trap sizes to probe the small-k regime and thereby determine $d\bar{B}/dk$ and $d^2\bar{B}/dk^2$. Currently, typical particle radii in the experiments range from about 0.1 to 0.2 μm and trap sizes are on the order of 1 μm, and so $k\sigma \approx 0.6$–1.2. It is also, of course, possible to tune the reduced wave number by varying particle size.

APPENDIX

The integrals required in Sec. II can be performed by starting with a generating integral

$$J(kr) = \int_0^\pi d\theta \cos(kr\cos\theta)\sin\theta = \frac{2\sin kr}{kr} = 2j_0(kr), \tag{A1}$$

where $j_0(kr)$ is a spherical Bessel function. The integrals needed in Sec. II, done with the generating integral above, are given by

$$\begin{aligned} I_1(kr) &= \int_0^\pi d\theta[1-\cos(kr\cos\theta)]\sin\theta\cos^2\theta \\ &= \frac{2}{3} - \left(\frac{4\cos kr}{k^2r^2} + \frac{2(k^2r^2-2)\sin kr}{k^3r^3}\right), \end{aligned} \tag{A2}$$

$$\begin{aligned} I_2(kr) &= \int_0^\pi d\theta[1-\cos(kr\cos\theta)]\sin^3\theta \\ &= 4\left(\frac{1}{3} + \frac{\cos kr}{k^2r^2} - \frac{\sin kr}{k^3r^3}\right), \end{aligned} \tag{A3}$$

$$\begin{aligned} I_3(kr) &= \int_0^{2\pi}\int_0^\pi d\phi\, d\theta[1-\cos(kr\cos\theta)] \\ &\quad\times \sin\theta(1-\sin^2\theta\cos^2\phi) \\ &= 4\pi\left(\frac{2}{3} - \frac{\cos kr}{k^2r^2} + \frac{(1-k^2r^2)\sin kr}{k^3r^3}\right), \end{aligned} \tag{A4}$$

$$\begin{aligned} I_4(kr) &= \int_0^{2\pi}\int_0^\pi d\phi\, d\theta[1-\cos(kr\cos\theta)] \\ &\quad\times \sin^3\theta\cos^2\phi(1+\sec^2\theta) \\ &= \frac{2\pi}{3}\left[4 - \left(3+\frac{6}{k^2r^2}\right)\cos kr + \frac{6\sin kr}{k^3r^3}\right. \\ &\quad \left. - \frac{3\sin kr}{kr} - 3kr\,\mathrm{Si}(kr)\right], \end{aligned} \tag{A5}$$

where Si is the sine integral. One finds that $krI_1'(kr) \sim -2\cos kr$ and $krI_2'(kr) \sim -\sin kr/kr$.

ACKNOWLEDGMENT

The authors would like to acknowledge many helpful discussions with Dr. Joseph Junio.

[1] R. Venkatesh and R. V. Gopala Rao, J. Phys. Chem. **98**, 9153 (1994).
[2] S. H. Chen, *Physical Chemistry—An Advanced Treatise* (Academic, New York, 1971).
[3] T. M. A. Khajil, J. Phys. I **5**, 1223 (1995).
[4] J. Junio, S. Park, M.-W. Kim, and H. D. Ou-Yang, Solid State Commun. **150**, 1003 (2010).
[5] R. Castañeda Priego, A. Rodríguez-Lopéz, and J. M. Méndez-Alcaraz, J. Phys. Condens. Matter **15**, S3393 (2003).
[6] S. Asakura and F. Oosawa, J. Chem. Phys. **22**, 1255 (1954).
[7] R. Dickman, P. Attard, and V. Simonian, J. Chem. Phys. **107**, 205 (1997).
[8] J. C. Crocker, J. A. Matteo, A. D. Dinsmore, and A. G. Yodh, Phys. Rev. Lett. **82**, 4352 (1999).
[9] T. Biben, P. Bladon, and D. Frenkel, J. Phys. Condens. Matter **8**, 10799 (1996).
[10] P. Schofield, Proc. Phys. Soc. **88**, 149 (1966).
[11] W. G. T. Kranendonk and D. Frenkel, Mol. Phys. **72**, 679 (1991).
[12] M. Dijkstra, R. van Roij, and R. Evans, Phys. Rev. Lett. **81**, 2268 (1998).

[13] J. P. Boon and S. Yip, *Molecular Hydrodynamics* (Dover, New York, 1980).
[14] A. Z. Akcasu and E. Daniels, Phys. Rev. A **2**, 962 (1970).
[15] D. Chandler, *Introduction to Modern Statistical Mechanics* (Oxford University Press, New York, 1987).
[16] A. Onuki, *Phase Transition Dynamics* (Cambridge University Press, Cambridge, 2004).
[17] P. Vashishta, R. K. Kalia, J. P. Rino, and I. Ebbsjo, Phys. Rev. B **41**, 12197 (1990).
[18] T. Boublik, I. Nezbeda, and K. Hlavatý, *Statistical Thermodynamics of Simple Liquids and Their Mixtures* (Elsevier, Amsterdam, 1980).
[19] N. F. Carnahan and K. E. Starling, J. Chem. Phys. **51**, 635 (1969).